



Variability and persistence of scour at bridges using stochastic simulations

Alonso Pizarro¹, Oscar Link², Demetris Koutsoyiannis³

¹Escuela de Ingeniería en Obras Civiles, Universidad Diego Portales, Santiago, 8370109, Chile

²Department of Civil Engineering, Faculty of Engineering, Universidad de Concepción, Edmundo Larenas 219, Concepción, 403000, Chile

³Department of Water Resources and Environmental Engineering, School of Civil Engineering, National Technical University of Athens, Zographou, Athens, 15772, Greece

10 *Correspondence to: Alonso Pizarro (alonso.pizarro@mail_udp.cl)*

Abstract. The stochastic and non-stochastic properties of the scouring process at bridges are analysed by coupling synthetic streamflow generations with a scour and fill model considering the upstream sediment supply. Streamflow was generated using the asymmetric moving-average (AMA) scheme that preserves the Hurst-Kolmogorov (HK) dynamics, the second-order dependence structure, time asymmetry, and the first four statistical moments of the marginal distribution. Stationarity, 15 homogeneity, and ergodicity of the streamflow and scouring processes were assumed. Monte Carlo analyses covered 12,000 realisations for each of the three considered scenarios with different upstream sediment supply. Extreme scour events were assessed using annual maxima with GEV fitting and compared against the equilibrium scour. The dependence structure was identified with the climacogram and climacospectrum stochastic tools and fitted with a filtered HK model (FHK-CD). The obtained results show a multi-scale dynamics of the scouring process with rough and weak persistent behaviour ($M \approx 0.40$; 20 $H \approx 0.60$), while envelopes span from antipersistent to strongly persistent scour regimes (H up to ≈ 0.86) depending on the upstream sediment supply. It is worth noting that the upstream sediment supply reduced the envelope variability and modified the extreme scour values. Additionally, synchronisation between extreme events of streamflow and scour showed a weak correspondence (Critical Success Index $\approx 0.15 - 0.60$), indicating that streamflow extremes do not systematically translate into scour extremes. Finally, scour depths with a given return period (computed from scour time series) increase 25 with upstream sediment supply.

1 Introduction

Scour continues to be a leading cause of infrastructure damage worldwide. Local scour – occurring at pipelines, bridge piers, groynes, and abutments – is a highly time-dependent process driven by non-linear interactions among the fluid, the turbulent flow, the sediment dynamics, and the geometry of the obstacle opposing the flow (Breusers et al., 1977; Dargahi, 1990; 30 Raudkivi, 1986). The interplay between scour and fill results in significant temporal variability in scour depth and bed level (Lee et al., 2021; Link et al., 2020; Lu et al., 2008; Pizarro et al., 2020), making the accurate prediction of extreme scour



depths a crucial aspect of bridge safety. Current design practices typically adopt enveloping equilibrium scour curves based on the magnitude of extreme streamflow events, which usually have return periods of 100-200 years (see, e.g.: Arneson et al., 2012; Chilean Ministry of Public Works (MOP), 2020; German Association for Water, Wastewater and Waste (DWA), 2020; Melville and Coleman, 2000). Although these approaches provide conservative safety margins (Rifo et al., 2022; Shahriar et al., 2021), failures still occur under scattered peak flood events (Cook et al., 2015), evidencing the stochastic nature of scouring processes and the limitations of adopted design philosophies.

Hydrological processes exhibit intrinsic variability and persistence at multiple temporal scales (Dimitriadis et al., 2021a; Koutsoyiannis, 2010, 2011). Long-term persistence (LTP) clusters extreme events over decades, substantially increasing uncertainty in design (Koutsoyiannis and Montanari, 2007), while short- and intermediate-term persistence (STP and ITP) control variability at local and seasonal scales. These properties challenge the reliability of return-period-based designs, which assume that extreme events are independent of each other. Moreover, streamflow records are often sparse, difficult to measure during floods, and subject to errors in rating curves, further propagating uncertainty in scour estimates.

Probabilistic approaches have therefore been proposed to incorporate hydrologic uncertainty into scour predictions (Brandimarte et al., 2006; Johnson, 1992). Monte Carlo frameworks have been utilised to integrate flow variability with equilibrium scour equations, providing practical guidance for engineering design. However, these methods remain time-independent, neglecting the inherently dynamic nature of scour. Time-dependent models (such as SRICOS, Briaud et al., 2007) have enabled the simulation of scour evolution under variable hydrographs; however, their lack of representation of sediment deposition leads to unrealistic continuous and monotonically increasing scour growth. More recently, advanced models (see, e.g., Flores-Vidriales et al., 2022, and Link et al., 2017, as well as Pizarro et al., 2017a with fill model extension) have incorporated both time dependence and depositional processes, opening the possibility of more physically consistent probabilistic frameworks.

Despite these advances, fundamental research questions remain unresolved: What are the stochastic and non-stochastic properties of the scouring process? Is time asymmetry a significant concern for bridge scour? Is there a direct correspondence between extreme events of streamflow and scour? Stochastic frameworks that consider hydrological variability, capture time asymmetry, and generate long synthetic scour records can contribute to answering these questions.

The present study addresses the aforementioned knowledge gaps by coupling stochastic simulations of river streamflow with a deterministic scour and fill model that accounts for upstream sediment supply. Streamflow time series are generated using the asymmetric moving average (AMA) scheme, which parsimoniously preserves the first four statistical moments, second-order dependence structure, and time asymmetry. These are then propagated through time-dependent scour models to produce synthetic scour series suitable for extreme value analysis. We evaluate the stochastic properties of the scouring process, assess the role of time asymmetry, and quantify uncertainty in design scour estimation. The rest of this document is



organised as follows: the case study and methodology for stochastic and pier-scour analysis are presented in Section 2; Section 3 shows the results; Section 4 addresses strengths and limitations, whereas conclusions are provided at the end.

65 2 Methods

2.1 River streamflow data and bridge case study

Streamflow data from the “Trancura River before the Llafenco River” gauging station was selected (ID: 09414001) due to the near-natural hydrologic regime and data monitoring frequency. Its catchment is located in Southern Chile (lat: 39.33 S, lon: 71.77 W), and considers only near-natural flow conditions, neither altered through hydropower plants nor lake regulation or water transfer. The catchment area is 1380 km², the mean annual precipitation is 2853 mm, and the aridity index is 0.3. The maximum, mean, and outlet catchment elevations are 3746, 1147, and 363 m a.s.l., respectively. The gauging station covers several decades of monitoring, but the period from 23/11/2001 to 31/01/2024 was selected for analysis due to its hourly measurement frequency (resulting in a total of 181,038 non-empty values). This temporal scale is crucial to characterise hydrological dynamics in terms of magnitude, frequency, duration, timing, and rate of change. Additionally, the computing of the effective flow work parameter (W^* , see subsection 2.3.1) is very sensitive to this time discretisation, in which a more accurate hydrograph representation leads to a more accurate calculation. Figure 1 shows the catchment location and two hydrological years of stream flows, whereas Table 1 shows 12 hydrological signatures that characterise hydrological dynamics.

The case study consists of a two-span bridge (60 m long) with one submerged pier (the bridge span is 30 m). The bridge pier is cylindrical with a diameter of 2.5 m. The river cross-section has an average width of 50 m. The riverbed was composed of non-uniform gravels, with a d_{50} of 41.6 mm and a d_{90} of 100.2 mm. Table 2 shows the grain size distribution of the riverbed sediments.

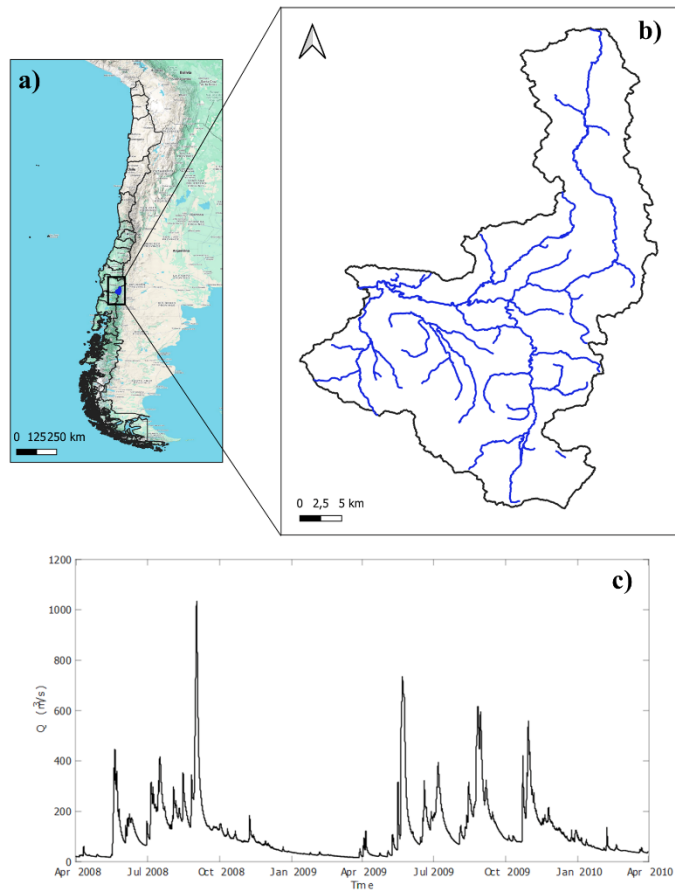


Figure 1: Location of the analysed catchment (Fig. 1a, b) and streamflow data visualisation (Fig. 1c) of two hydrological years (2008 and 2009). Notice that the hydrological year starts on the 1st of April.



Table 1: Hydrological signatures characterising the magnitude, frequency, duration, timing, and rate of change of streamflow.

	Hydrological Signature	Description	Value	Dimensional units
Magnitude	Q_{mean}	Mean streamflow value	6.714	mm/d
	Q_5	5-th streamflow percentile	1.785	mm/d
	Q_{95}	95-th streamflow percentile	17.038	mm/d
	BFI	Baseflow index	0.732	-
Frequency	HighQFreq	High Q frequency	0.002	-
	LowQFreq	Low Q frequency	0.017	-
Duration	HighQDur	High Q duration	1.583	d
	LowQDur	Low Q duration	12.143	d
Timing	HFD	Half flow date	147	date
	HFI	Half flow interval	122	d
Rate of change	AC1	Lag-1 autocorrelation	0.934	-
	Slope FDC	Slope of the flow duration curve	-2.338	-

Table 2: Grain size distribution of the riverbed sediments.

Grain Size (mm)	Percent finer (%)
112.0	97%
80.0	80%
56.0	66%
40.0	48%
28.0	32%
20.0	17%
12.0	9%
7.4	5%
5.4	4%
3.0	3%
1.5	2%
0.8	0%
0.4	0%



2.2 Stochastic streamflow analysis and synthetic time series generation

90 The dependence structure of the river streamflow process was modelled in terms of the climacogram stochastic tool (see Dimitriadis et al., 2021b; Dimitriadis and Koutsoyiannis, 2015; Koutsoyiannis, 2010), defined as the variance $\gamma(k)$ of the averaged process $\underline{z}(t)$ depending on the averaging time scale k . The climacogram is useful for detecting and evaluating LTP dynamics. For STP and ITP, the climacospectrum stochastic tool is used. Such a stochastic tool was recently introduced by Koutsoyiannis (2016, 2024), having, in most cases, the same asymptotic behaviour and properties as the power spectrum, but
 95 is computed only in terms of variances. Consequently, it presents less biased results, making it more convenient for model fitting and identification (Koutsoyiannis, 2016). Table 3 presents the mathematical expressions for the climacogram and climacospectrum stochastic tools

Table 3: Definition of the stochastic tools and notations used for stochastic processes.

	Definition and Notation	Observations	Equation number
Time	t		
Time Scale	k		
Stochastic process	$\underline{z}(t)$	Assumed stationary	
Cumulative stochastic process	$\underline{Z}(t) = \int_0^t \underline{z}(\xi) d\xi$	Nonstationary	(1)
Climacogram	$\gamma(k) = \text{Var} \left[\frac{(\underline{Z}(t+k) - \underline{Z}(t))}{k} \right]$	$\gamma(0) = \text{Var}[\underline{x}(t)]$	(2)
Climacospectrum	$\psi(k) = \frac{k(\gamma(k) - \gamma(2k))}{\ln 2}$		(3)

100 A parsimonious stochastic model was used to fit the dependence structure of the river streamflow process in terms of the climacogram (Filtered Hurst-Kolmogorov model with a generalised Cauchy-Dagum-type climacogram, FHK-CD). The FHK-CD model is general and flexible for any process, regardless of whether the process is rough or smooth, persistent or antipersistent. It has six fitting parameters and can model the dependence structure from small to large temporal scales:



$$\gamma(k) = \lambda_1^2 (1 + (k/\alpha_1)^2)^{H-1} + \lambda_2^2 (1 - (1 + (k/\alpha_2)^{-2})^{-M}) \quad (4)$$

where λ_1 and λ_2 are scale parameters with dimensions of $[x^2]$, α_1 and α_2 are scale parameters with dimensions of $[t]$, and M and H are the fractal and Hurst parameters, respectively. It is worth mentioning that M and H are dimensionless, ranging between 0 and 1, and determine the local and global dependence structure. Eq. (4) can be simplified, when parsimony is sought, by setting $\lambda_1 = \lambda_2 = \lambda$ and $\alpha_1 = \alpha_2 = \alpha$. Therefore, the FHK-CD model with four parameters is presented in Eq. (5):

$$\gamma(k) = \lambda^2 (1 + (k/\alpha)^2)^{H-1} + \lambda^2 (1 - (1 + (k/\alpha)^{-2})^{-M}) \quad (5)$$

The variance estimator for the climacogram and climacospectrum can be computed as:

$$\hat{\gamma}(k) = \frac{1}{[n/\kappa]} \sum_{i=1}^{[n/\kappa]} \left(\underline{z}_i^{(\kappa)} - \hat{\mu} \right)^2 \quad (6)$$

where $\kappa = k/\Delta$ is the dimensionless time scale, Δ is the time resolution at each sample time series, $[n/\kappa]$ is the integer part of n/κ , and $\underline{z}_i^{(\kappa)}$ is the i th element of the averaged sample of the process at scale κ , i.e.:

$$\underline{z}_i^{(\kappa)} = \frac{1}{\kappa} \sum_{j=(i-1)\kappa+1}^{i\kappa} z_j \quad (7)$$

It is worth mentioning that the bias of variance estimator presented in Eq. (6) can be easily computed by Eq. (8). Additionally, and for fitting purposes, the standardised climacogram ($\hat{\gamma}(k)/\hat{\gamma}(1)$) and climacospectrum ($\hat{\psi}(k)/\hat{\psi}(1)$) are used. The effect of the annual cycle was removed following Koutsoyiannis (2019, 2020), i.e. multiplying 12 coefficients (one per month and summing 1 in total) by the streamflow values. The value of the coefficients was found by minimising the variance of the transformed time series.

$$E[\hat{\gamma}(k)] = \gamma(k) - \gamma([n/\kappa]k) \quad (8)$$

For synthetic generation purposes, the asymmetric-moving-average (AMA) scheme is adopted (see Koutsoyiannis, 2019, 2020)). The AMA scheme can explicitly preserve any arbitrary second-order dependence structure, as long as a mathematical expression for it exists. The marginal distribution function of the generated data approximates the original one through the statistical moments of the process. In this study, the first four moments are preserved, enabling a good approximation of the original marginal distribution function as was shown in Dimitriadis and Koutsoyiannis (2018). Therefore, the approximation can be carried out with controlled accuracy. The AMA scheme generates \underline{z}_i by



$$\underline{z}_i = \sum_{j=-J}^J a_j \underline{v}_{i-j} \quad (9)$$

where a_j are coefficients (weights) computed from the autocovariance function and \underline{v}_i is white noise. Notice that J is theoretically infinite, although for simulation purposes J is taken as a large integer providing negligible truncation errors
 125 (Koutsoyiannis, 2000). A generic solution for a_j was proposed by Koutsoyiannis (2020):

$$a_j = \int_{-1/2}^{1/2} e^{2\pi(\theta(\omega)-j\omega)} A^R(\omega) d\omega \quad (10)$$

where $\theta(\omega)$ is any real function having the following property $\theta(-\omega) = -\theta(\omega)$ and $A^R(\omega) = \sqrt{2s_d(\omega)}$.

Time asymmetry is handled through the preservation of the skewness ratio between the differenced process $\tilde{z}_\tau (= \underline{z}_\tau - z_{\tau-1})$ and the original one \underline{z}_τ ,

$$\frac{\tilde{C}_s}{C_s} = \frac{\sum_{j=-J}^J (a_j - a_{j-1})^3}{\left(\sum_{j=-J}^J (a_j - a_{j-1})^2\right)^{3/2}} \frac{\left(\sum_{j=-J}^J a_j^2\right)^{3/2}}{\sum_{j=-J}^J a_j^3} \quad (11)$$

where \tilde{C}_s is the skewness of the differenced process \tilde{z} and C_s is the skewness of the original process \underline{z}_τ . Note that the
 130 skewness ratio depends only on the a_j sequence, and as a consequence, it depends on the (a)symmetric parameter $\theta(\omega)$.
 Interesting the fact that $\theta(\omega) = 0$ implies time symmetry and AMA converges to the symmetric moving average (SMA)
 scheme. However, $0 < \theta(\omega) \leq 1/4$ preserves time asymmetry. As a consequence, $\theta(\omega)$ must be chosen to preserve the
 skewness ratio. Figure 2 shows an example of synthetically generated streamflow using AMA with two different θ values.
 Notice that $\theta = 0.00$ generates symmetric-to-the-peak time series, whereas $\theta = 0.10$ generates positively asymmetric time
 135 series.

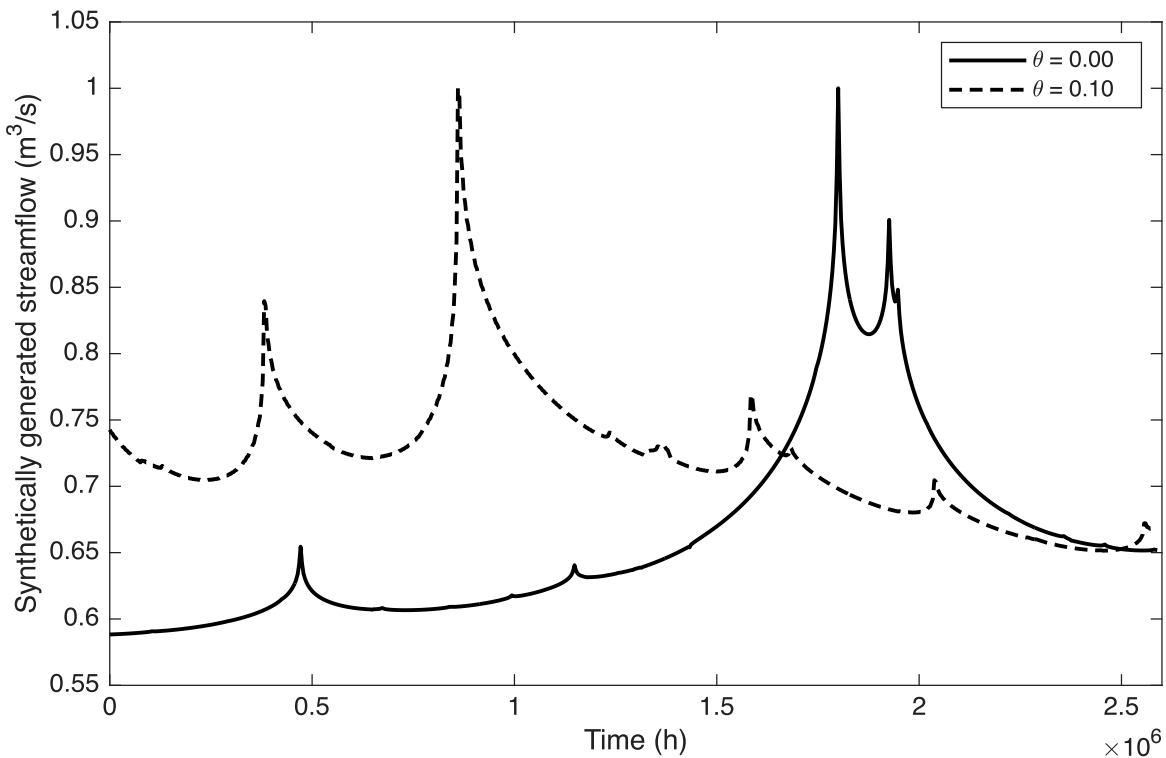


Figure 2: Example of synthetically generated streamflow using AMA with two different θ values. Notice that $\theta = 0.00$ generates symmetric-to-the-peak time series, whereas $\theta = 0.10$ generates positively asymmetric time series. Generator setup: $M = 0.54$; $H = 0.64$; $\alpha = 486$ (h); mean, variance, skewness, and kurtosis were $30 \text{ m}^3/\text{s}$, $10 \text{ m}^6/\text{s}^2$, 10 , 4 , respectively. Plotted Q is the standardised synthetically generated streamflow, i.e. $Q / \max(Q)$.

140

2.3 Computation of time-dependent local scour and fill at a bridge pier

The bridge-pier scour entropic (BRISENT) model is considered for time-dependent scour analysis because of its flexibility and parsimonious modelling within time-dependent hydraulic conditions (Pizarro et al., 2017a). BRISENT relies on the principle of maximum entropy and on the effective flow work parameter, W^* (Pizarro et al., 2017b), which accounts for the 145 influence of flood waves on the local scour process. W^* is mathematically defined as follows:

$$W^*(t_{\text{con}}) = \int_0^{t_{\text{con}}} \frac{1}{t_R} \left(\frac{u(t) - 0.5u_c}{u_R} \right)^4 \delta dt \quad (12)$$

where t_{con} is the considered time, t_R is a reference time defined as z_R/u_R , $z_R = D^2/2d_{50}$ is a reference length (D is the pier-diameter and d_{50} the sediment-size), $u(t)$ is the time-dependent section averaged flow velocity, u_R is a reference velocity (=



150 $\sqrt{\rho' g d_{50}}$, where $\rho' = (\rho_s - \rho_w)/\rho_w$ is the relative density between sediment “s” and water “w”, and g is the gravitational acceleration). u_c is the critical flow velocity for incipient motion of sediment particles and δ is an on-off step function defined as:

$$\delta = \begin{cases} 0, & u(t)/u_c < 0.5 \\ 1, & u(t)/u_c \geq 0.5 \end{cases} \quad (13)$$

The BRISENT model has three fitting parameters (λ , W_{\max}^* , and S) and their empirical expressions rely on a large laboratory dataset with a wide range of key dimensionless parameters which control the scour process. BRISENT is presented in Eq. (14), while from Eq. (15) to Eq. (17) are the empirical expressions for the fitting parameters.

$$Z^* = \frac{1}{\lambda} \ln \left\{ 1 + \frac{W^*}{W_{\max}^*} [\exp(S) - 1] \right\} \quad (14)$$

$$\lambda = 4.237 \left(\frac{D}{d_{50}} \right)^{0.957} \quad (15)$$

$$W_{\max}^* = \exp \left[21.84 \left(\ln \frac{D}{d_{50}} \right)^{-0.295} \right] \quad (16)$$

$$S = \frac{21.185 (D/d_{50})^{0.957}}{0.4(D/d_{50})^{1.2} + 10.6(D/d_{50})^{-0.13}}. \quad (17)$$

155 The scour hole refilling process was considered, following Link et al. (2020), i.e., sediment deposition occurring during the falling limb of the hydrograph. The time-dependent sediment deposition rate, $d(t)$, was computed as

$$d(t) = \alpha_d \frac{w_s}{q(t)} (g_s(t) - g_s^*(t)) \quad (18)$$



where, α_d is considered a constant ($= 0.5$ according to Link et al., 2020; Pizarro et al., 2022), w_s is the sediment falling velocity, $q(t)$ is the specific discharge per unit width, $g_s(t)$ is the sediment supply rate (kg/m/s), and $g_s^*(t)$ is the sediment transport capacity (kg/m/s) estimated using the Meyer-Peter and Müller (1948) equation:

$$g_s^* = 8\rho_s(\rho' g d_s^3)^{0.5} \left[\left(\frac{C_R}{C'_R} \right)^{1.5} \theta - \theta_c \right]^{1.5} \quad (19)$$

160 where C_R is the total Chézy coefficient due to effective bed roughness k_s ($= 18 \log(12h/k_s)$), C'_R is the Chézy coefficient due to particle roughness d_{90} ($= 18 \log(12h/d_{90})$), and θ and θ_c are the Shields and threshold Shields parameters.

The presented deposition modelling framework considers sediment deposition if the hydrograph is in the falling limb and $g_s(t) > g_s^*(t)$. $g_s(t)$ is estimated as $g_s^*(t)$ evaluated in the previous instant, i.e. $g_{s[i]} = \xi g_{s[i-1]}$, where ξ is an exceedance sediment supply coefficient and i reports the discrete time instant. In consequence, the sediment deposition depth is 165 calculated through a fractional transport formulation as follows:

$$d_{[i]} = \frac{\alpha_d}{\rho_s(1-p)} \sum_{j=1}^n \frac{w_{s[j]} P_{[j]}}{q_{[i]}} \left(\xi g_{s[i-1,j]}^* - g_{s[i,j]}^* \right) \Delta t \quad (20)$$

where j is a counter for the considered sediment sizes in the granulometric curve, ρ_s is the sediment density, p is the sediment porosity, and $P_{[j]}$ is the percentage of the soil which contains the sediment size $d_{s[j]}$. Therefore, the scour depth considering the refilling scour process is computed as $z_{[i]} = z_{\text{scour}_{[i]}} - d_{[i]}$ and $W_{[i]}^* = W_{\text{scour}_{[i]}}^* - \Delta W_{d_{[i]}}^*$. The scour and deposition models were implemented in a software package, and a sensitivity analysis of their parameters was presented by 170 Pizarro et al. (2022). Figure 3 shows an example of scour depth time series computed with the scour and fill models. It is worth mentioning that erosional and sediment (re)deposition dynamics are captured by the simulation.

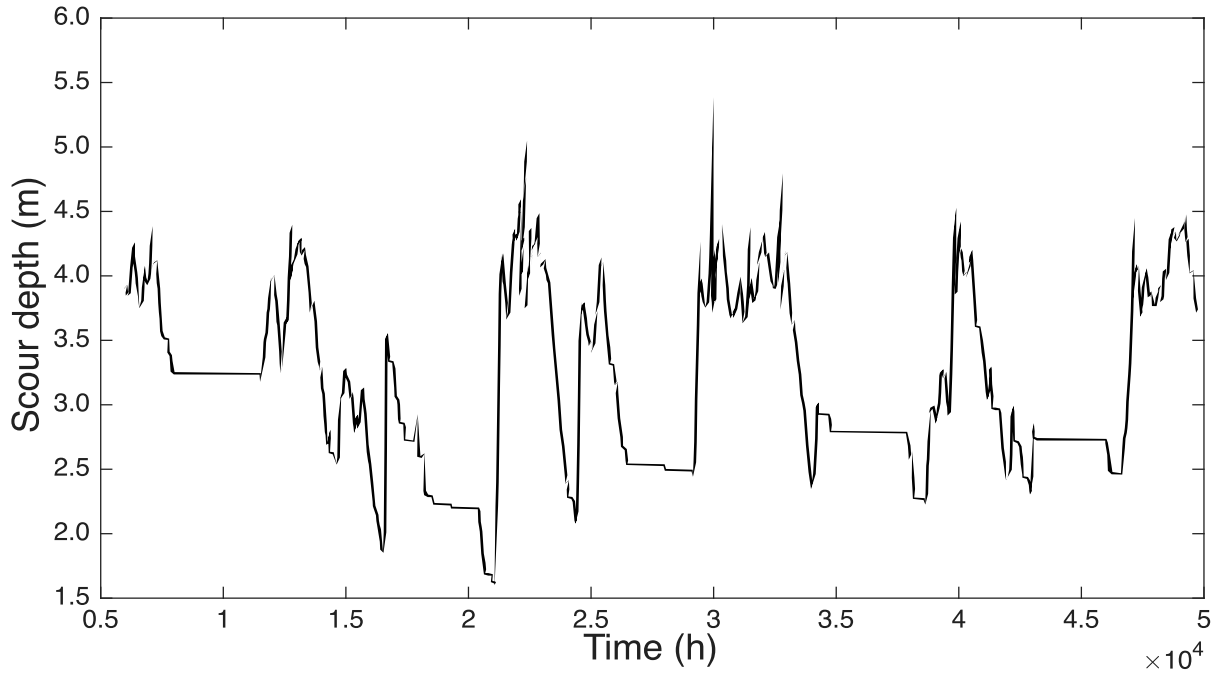


Figure 3: Example of scour depth time series using the scour and fill model.

Equilibrium scour (z_{eq}) is computed with the widely used scour equation by Sheppard et al. (2014):

$$\frac{z_{\text{eq}}}{a^*} = 2.5f_1f_2f_3 \quad \text{for } 0.4 \leq \frac{u}{u_c} < 1.0 \quad (21)$$

$$\frac{z_{\text{eq}}}{a^*} = f_1 \left[2.2 \left(\frac{\frac{u}{u_c} - 1}{\frac{u_{1p}}{u_c} - 1} \right) + 2.5f_3 \left(\frac{\frac{u_{1p}}{u_c} - u}{\frac{u_{1p}}{u_c} - 1} \right) \right] \quad \text{for } 1.0 < \frac{u}{u_c} < \frac{u_{1p}}{u_c} \quad (22)$$

$$\frac{z_{\text{eq}}}{a^*} = 2.2f_1 \quad \text{for } \frac{u}{u_c} > \frac{u_{1p}}{u_c} \quad (23)$$

$$u_{1p1} = 5u_c \quad (24)$$

$$u_{1p2} = 0.6\sqrt{gy_1} \quad (25)$$

$$u_{1p} = \begin{cases} u_{1p1} & \text{for } u_{1p1} \geq u_{1p2} \\ u_{1p2} & \text{for } u_{1p1} < u_{1p2} \end{cases} \quad (26)$$



$$f_1 = \tanh \left[\left(\frac{h}{a^*} \right)^{0.4} \right] \quad (27)$$

$$f_2 = \left\{ 1 - 1.2 \left[\ln \left(\frac{u}{u_c} \right) \right]^2 \right\} \quad (28)$$

$$f_3 = \left[\frac{\left(\frac{a^*}{d_{50}} \right)}{0.4 \left(\frac{a^*}{d_{50}} \right)^{1.2} + 10.6 \left(\frac{a^*}{d_{50}} \right)^{-0.13}} \right] \quad (29)$$

175 **2.4 Extreme events detection and return periods**

To assess the correspondence between the detection of extreme events in streamflow and scour, the critical success index (CSI, see Eq. 30) was used. The CSI computed the number of hits (H), misses (M) and false alarm (F) events. Hits are defined as matching events identified for both streamflow and scour, whereas misses are events identified only for streamflow. False alarm events are those identified only for scour. CSI ranges between 0 and 1, with the latter the optimum 180 value. We defined hits as the scour events that overlap with the streamflow events by at least 70%. A tolerance of 2 hours before and 2 hours after the original event identification was considered, accounting for possible uncertainty in the event identification procedure. The threshold for streamflow and scour events identification was the 40th percentile of the annual maxima series.

$$\text{CSI} = \frac{H}{H + M + F} \quad (30)$$

185 Return periods of scour depths were computed directly from the scour time series using annual maxima series and fitting the Generalised Extreme Value (GEV) probability distribution function.

2.5 Monte Carlo simulations

Monte Carlo analysis was performed with N = 12,000 simulations, each of them with 60 years at an hourly temporal scale of the synthetic generated streamflow time series. These simulations were used as input for the time-dependent scour and fill model, generating the same number of scour time series. Additionally, and with the intention to assess the effect of upstream 190 sediment supply on scour (and, therefore, the sediment deposition effect), three different cases were investigated: i) $\xi = 1.0$; ii) $\xi = 1.5$; and, iii) $\xi = 2.0$. The latter cases range from sediment rates equal to the transport capacity (i.e., $\xi = 1.0$) to sediment supply exceeding the transport capacity (i.e., $\xi = 1.5$ and $\xi = 2.0$). In total, 36,000 simulations (12,000 for each ξ case) were performed.



2.6 Methodology outline summary

195 The methodology employed in this work encompasses the stochastic analysis of the Trancura River gauging station and the synthetic generation of river streamflow time series, which preserves time asymmetry, the second-order dependence structure, and the probability density function (through the first four statistical moments). Synthetic streamflow time series were replicates of the historical record and the inputs for the time-dependent scour and fill model. Monte Carlo analysis was performed with $N = 12,000$ simulations, each of them with 60 years at an hourly temporal scale of the synthetic generated
200 streamflow time series and scour time series. Three different cases of upstream sediment supply having a sediment rate equal to the transport capacity (i.e., $\xi = 1.0$) and sediment supply 50 and 100% higher than the transport capacity (i.e., $\xi = 1.5$ and $\xi = 2.0$, respectively). The stochastic properties of the scouring process were quantified in terms of the second-order dependence structure, the Hurst and Mandelbrot parameter, and time asymmetry through the skewness of the differenced process. The non-stochastic properties of the scouring process were quantified in terms of the CSI index and scour return
205 periods following Rifo et al. (2022).

2.7 Code availability

Codes for streamflow generation and scour computation were written in MATLAB and are available at Pizarro et al. (2025). In particular, the scripts consider the analysis and modelling of the river streamflow process, its synthetic generation (using the AMA scheme, which preserves time asymmetry, the second-order stochastic properties, and the first four statistical
210 moments), and the scour assessment following the methodology described above.

3 Results

3.1 Synthetic-generated streamflow coupled with scour and fill model

Figure 4 shows a representative example of the synthetically generated hourly streamflow series (orange) and the corresponding scour-depth response (blue) over a 60-year simulation period (one of the 36,000 simulations performed). As
215 shown in Fig. 4, the simulated streamflow time series exhibits pronounced variability, with recurrent peaks associated with high-flow events and recessions during lower-flow periods. These dynamics are consistent with the hydrological behaviour of the catchment. In this specific realisation, the maximum and median streamflow values reached 2299 and 94 m³/s, respectively, reflecting both the extreme events and the central tendency captured by the stochastic generator.

The blue curve shows the evolution of scour depth, computed by coupling the AMA-generated streamflow with the erosional
220 and fill model under the assumption of $\xi = 1.0$ (i.e., sediment supply equal to the transport capacity). The resulting scour-depth fluctuations showed deeper scour during high-magnitude streamflow peaks. Maximum and median scour depths for this simulation were 5.63 and 3.29 m, demonstrating the model's capacity to translate hydrological variability into



adjustments in sediment dynamics. Overall, Fig. 4 highlights the value of integrating stochastic flow generation with process-based scour modelling, enabling the exploration of long-term scour response under a wide ensemble of hydrological 225 conditions.

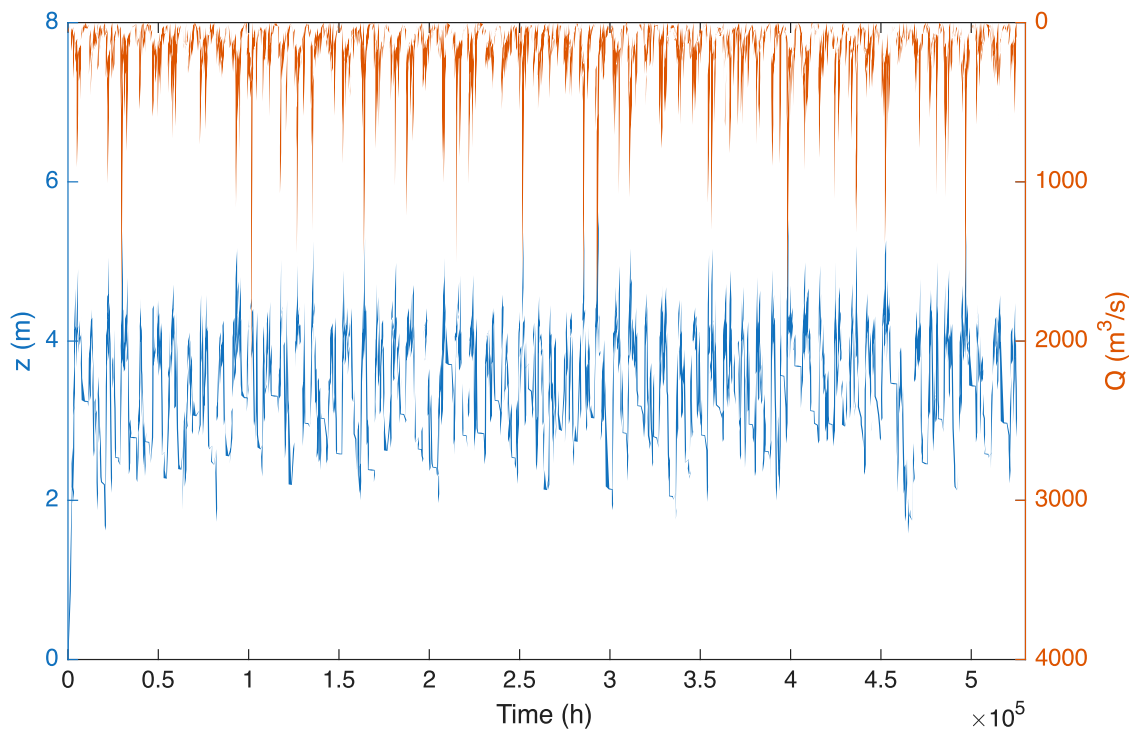
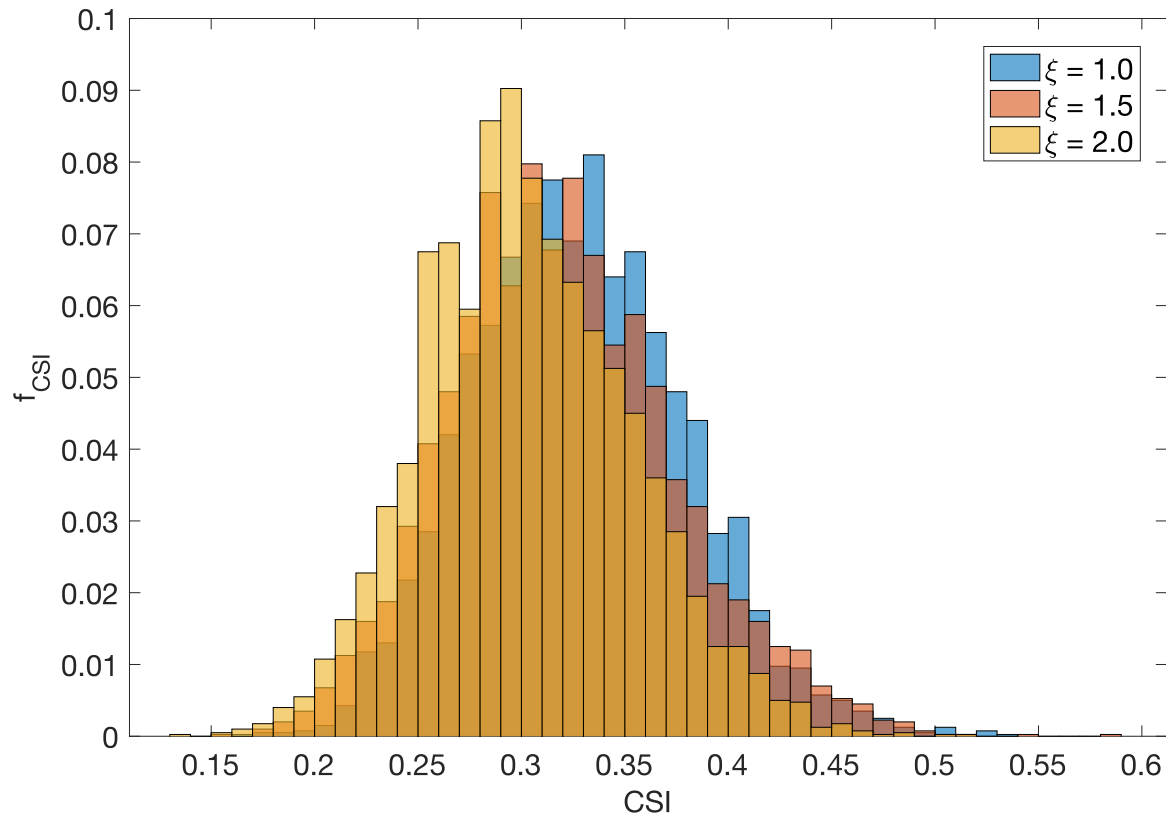


Figure 4: Synthetically generated hourly streamflow and corresponding scour depth over 60 years, considering $\xi=1.0$ (i.e., sediment rate equal to the transport capacity).

3.2 Non-stochastic properties of the scouring process

230 Non-stochastic properties of the scour process were assessed through the Critical Success Index (CSI) – between river streamflow and bridge scour – and the ratio between the magnitude of scour with a particular return period (computed from the scour simulations) and the equilibrium scour depth computed with the scour formula by Sheppard et al. (2014). Figure 5 shows that the three analysed cases (colours blue, red, and yellow are related to ξ values of 1.0, 1.5, and 2.0, respectively) yielded similar CSI values, ranging from approximately 0.15 to 0.60. A value of 0.15 means that only 15% of all identified 235 events occurred simultaneously for both river streamflow and scour. A trend from symmetric to positively asymmetric distribution of CSI's values for ξ equal 1.0 to 2.0 (CSI median values are 0.33, 0.32, and 0.30 for ξ equal 1.0, 1.5, and 2.0, respectively) is observed. It is worth mentioning that low CSI values mean a low correspondence between the occurrence of streamflow and scour events.



240

Figure 5: Histograms for the Critical Success Index (CSI) between river streamflow and bridge scour. Blue, red, and yellow colours are related to ξ equals to 1.0, 1.5, and 2.0.

Figure 6 shows the frequency distribution of the computed scour depth with $T = 100$ (blue), 150 (orange), 200 (yellow), and 300 (cyan) years for each scenario of upstream sediment supply with $\xi = 1.0, 1.5$, and 2.0 . The above-mentioned return 245 periods were selected due to their direct relationship with risk levels and design methods. In all cases, the scour depth to equilibrium scour depth ratio (z/z_{eq}) increased with ξ . In most analysed cases, scour depths computed with scour time series were higher than the equilibrium scour depth. Table 4 shows the exceedance probability for $z/z_{eq} > 1.0$.



Table 4: Exceedance probability for $z/z_{eq} > 1.0$ as a function of the considered return period and upstream sediment supply.
 250

ξ	Return Period			
	100	150	200	300
1.0	0	0	5.0×10^{-4}	0.0028
1.5	0.0040	0.0242	0.0568	0.1442
2.0	0.0076	0.0434	0.0950	0.2254

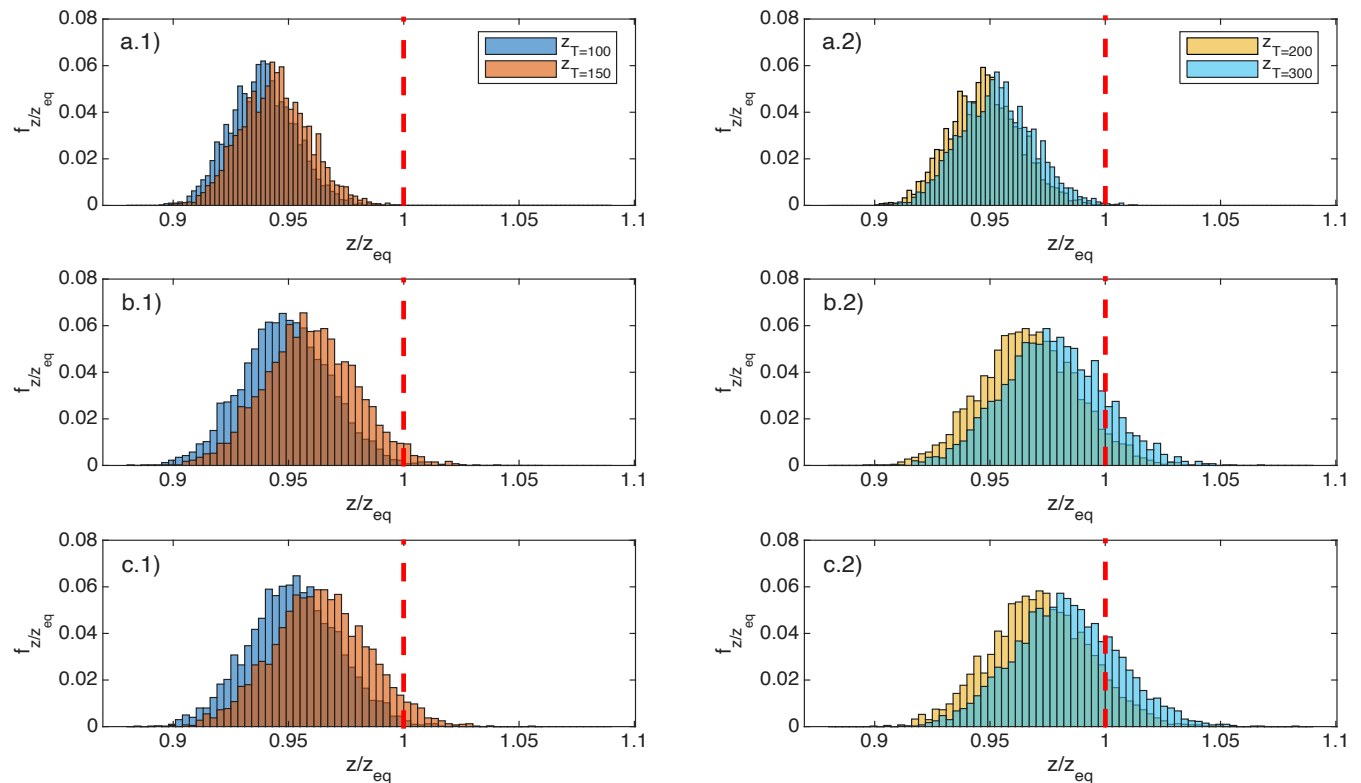


Figure 6: Scour depth to equilibrium scour depth ratio for different return periods and upstream sediment supply with $\xi = 1.0, 1.5$, and 2.0 . The red vertical dash lines are explicitly plotted at $z/z_{eq} = 1$.



255 **3.3 Stochastic properties of the scouring process**

The second-order dependence structure was quantified in terms of the climacogram and climacospectrum adapted for bias. All computations were standardised by dividing them by their first value. Only 90% of all available scales were used for model fitting purposes, mainly motivated by the high calculation uncertainty in small samples (i.e., with less than 10 values. See Dimitriadis and Koutsoyiannis, 2015). Figure 7 shows the envelope standardised climacograms as a function of $\xi = 1.0$ (red), 1.5 (blue), and 2.0 (black). It is worth noticing that the higher the ξ value, the narrower the envelopes; and, climacograms for $\xi = 1.5$ and $\xi = 2.0$ are similar.

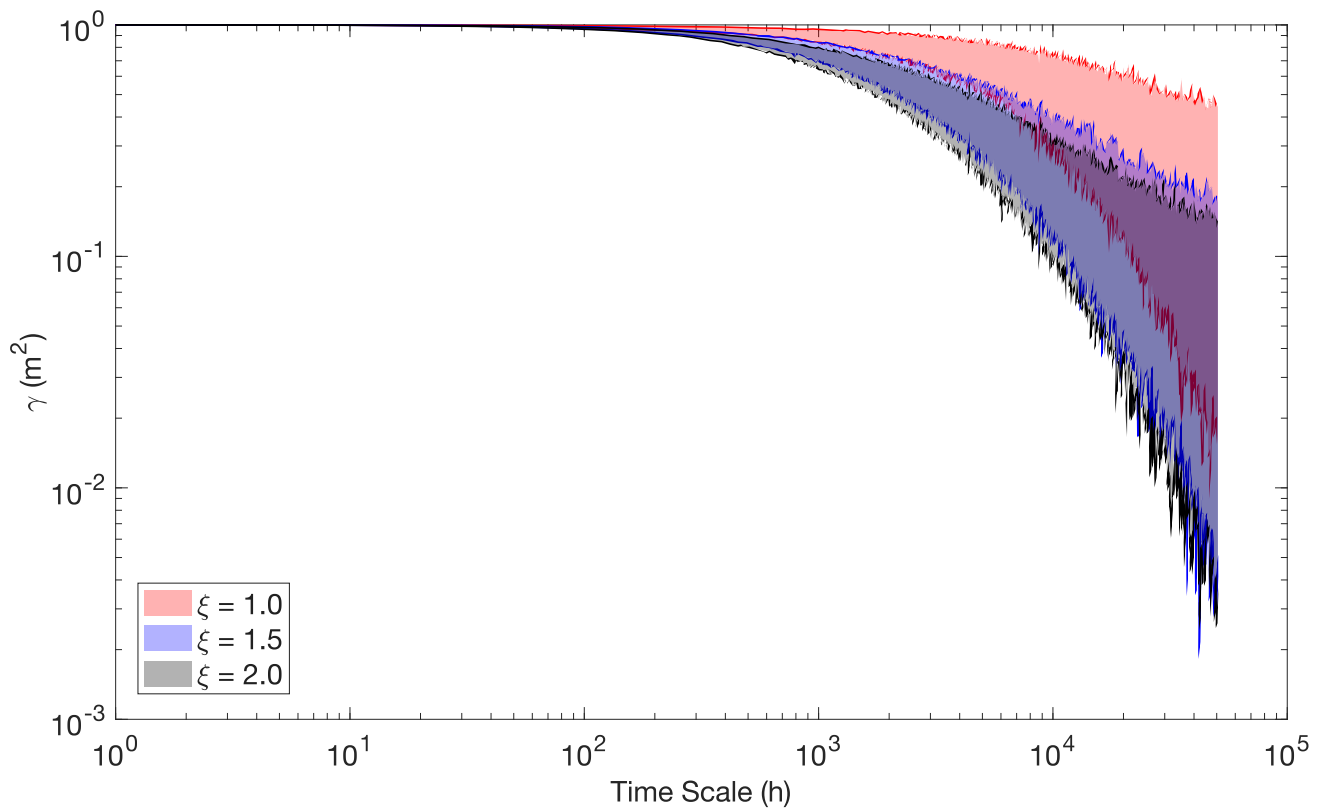


Figure 7: Envelope standardised climacograms for ξ equals to 1.0 (red), 1.5 (blue), and 2.0 (black). Each envelope takes into consideration 12000 scour simulations.

265 Figure 8 shows the mean standardised climacograms and climacospectrums for ξ equals to 1.0 (red), 1.5 (blue), and 2.0 (black). Mean standardised stochastic tools were considered as representative of the 12000 simulations. The continuous green line corresponds to the FHK-CD model. Interestingly, asymptotic dynamics at both small (assessed through the Mandelbrot parameter, M) and large (assessed through the Hurst parameter, H) temporal scales yielded similar values ($M \approx 0.40$ and $H \approx 0.60$). The latter is indicative of rough and (weak) persistent dynamics. Table 5 summarises these



270 asymptotic behaviours for the means and envelopes. Mean values are related to the mean standardised stochastic tool, while min and max correspond to the lower and upper envelopes.

Interestingly, and focusing on the envelopes, the strength of the Hurst dynamics of the scouring process depends on ξ , ranging from $H = 0.00$ (strong antipersistence dynamics) to $H = 0.86$ (strong LTP dynamics). On the other hand, the Mandelbrot parameter took values from 0.10 to 0.41 (i.e., having less variability than H). It is worth mentioning that rough 275 dynamics (i.e., $M < 0.5$) instead of a smooth one (i.e., $M > 0.5$) is usual in many hydrological processes at the analysed hourly scale such as the cases of near-surface temperature, relative humidity, dew point, sea level pressure, wind speed, and precipitation (see, e.g., Dimitriadis et al., 2021b; Dimitriadis and Koutsoyiannis, 2018).

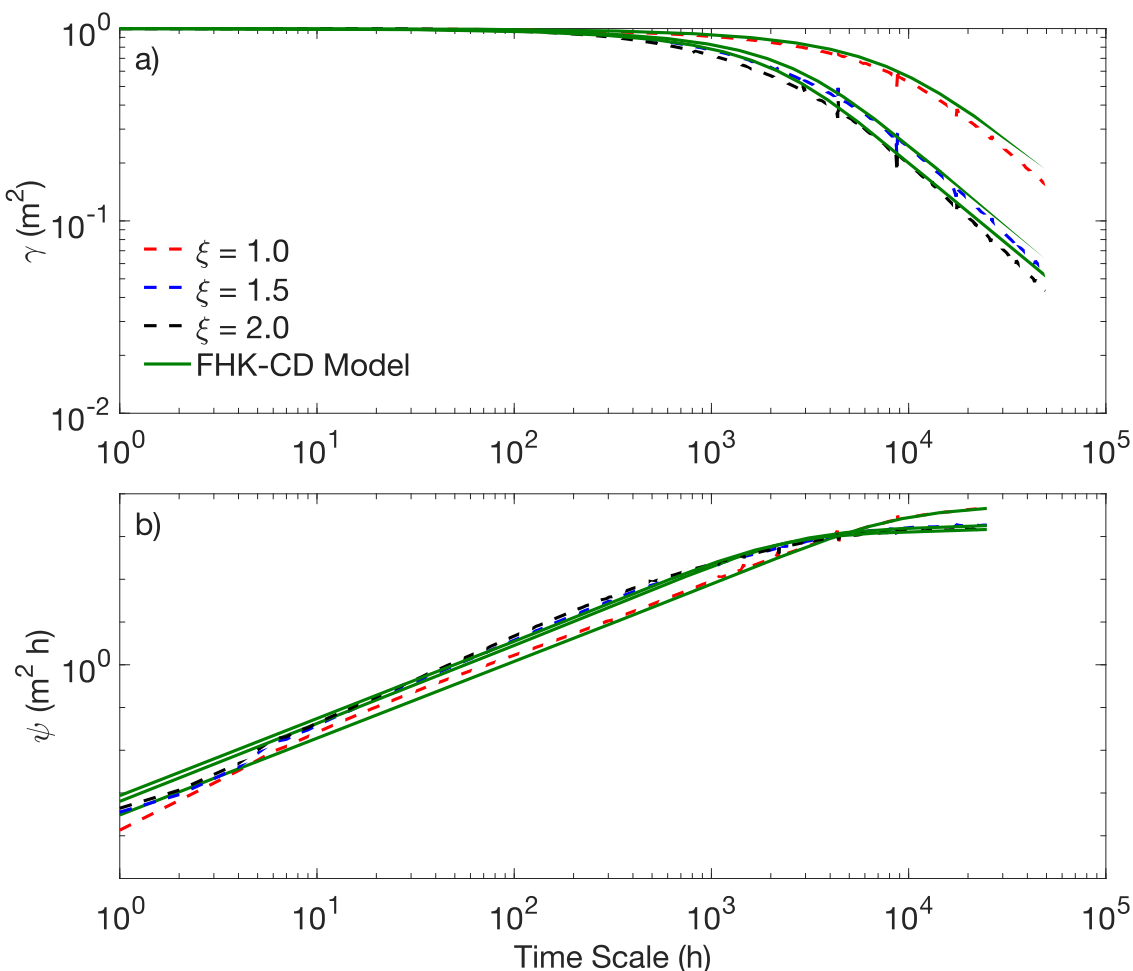


Figure 8: Mean standardised climacograms and climacospectrum for ξ equals to 1.0 (red), 1.5 (blue), and 2.0 (black).

280 The continuous green line is the FHK-CD model.



Table 5: Summary of asymptotic behaviours at small (M , Mandelbrot or fractal parameter) and large (H , Hurst parameter) scales. Mean values are related to the mean standardised stochastic tool, while min and max correspond to the envelopes. The minimum temporal scale under analysis was hourly.

ξ	Mean (rough persistent)		Min (rough antipersistent)		Max (rough persistent)	
	M	H	M	H	M	H
1.0	0.40	0.64	0.31	0.00	0.30	0.84
1.5	0.41	0.60	0.13	0.00	0.31	0.84
2.0	0.40	0.59	0.10	0.00	0.40	0.86

285 In terms of time asymmetry, the scour process showed negative skewness coefficients at short time scales, followed by a transition to positive values and convergence towards zero at longer time scales (see Fig. 9). This behaviour indicates that scour increments are not time-symmetric: large negative fluctuations dominate at fine resolutions, while positive dynamics emerge as aggregation increases. A systematic dependence of the scour depth on ξ , i.e. on the upstream sediment supply, was observed. For $\xi = 1.0, 1.5$, and 2.0 , the transition from negative to positive skewness occurred at approximately 195 (h),
 290 80 (h), and 54 (h), respectively. The subsequent return from positive to near-zero values occurred at around 20 000 (h), 6500 (h), and 5000 (h) for the same ξ values. These thresholds reveal that higher sediment availability reduces the persistence of asymmetry, leading to faster stabilisation of scour fluctuations.

The observed scale-dependent dynamics confirm that bridge scour cannot be described solely by equilibrium formulations, which ignore time asymmetry and stochastic persistence. Instead, our findings highlighted that skewness provides an
 295 additional diagnostic tool to assess the temporal structure of scour variability, especially in the presence of fill in the scour hole due to upstream sediment supply. Incorporating time asymmetry into stochastic frameworks, therefore, enhances the reliability of probabilistic scour hazard assessments.

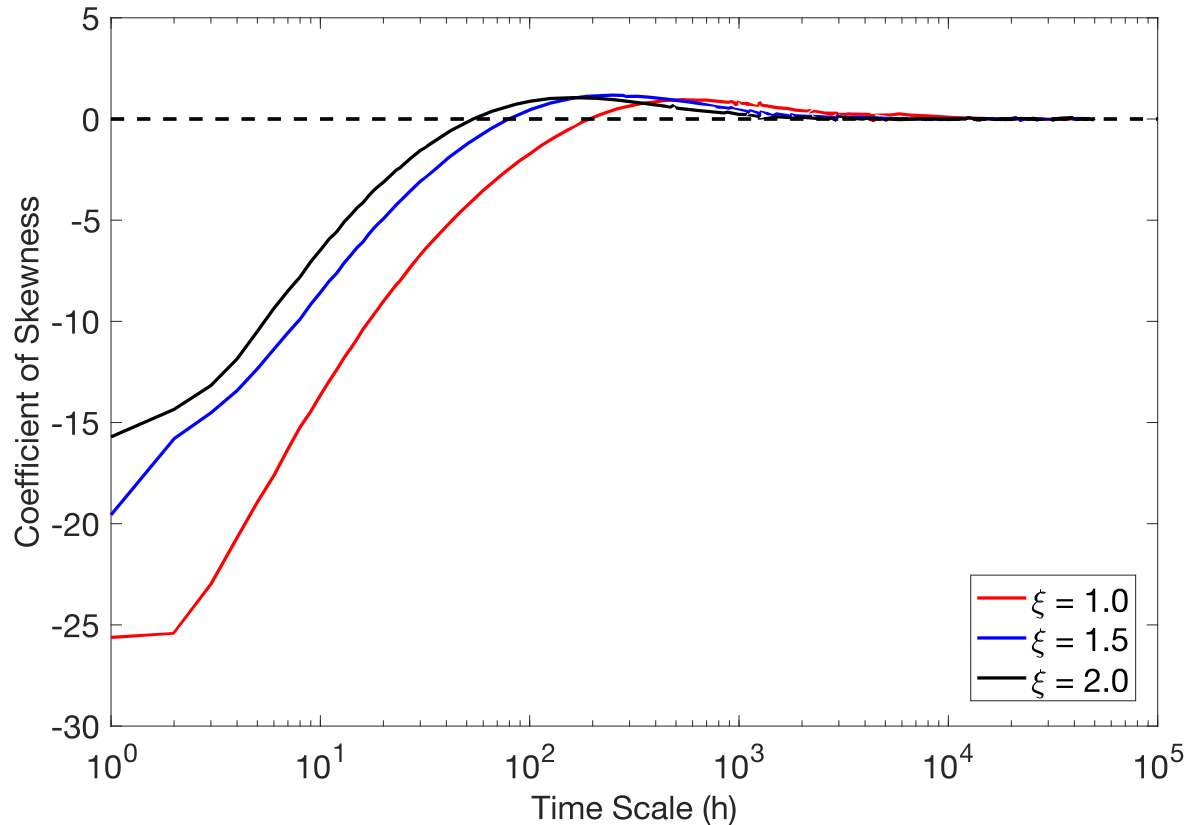


Figure 9: Skewness coefficient of the differenced scour time series as a function of the time scale. Plots refer to the 300 standardised series, which take the mean value of the 12,000 simulations. ξ equals to 1.0, 1.5, and 2.0 are related to the colours red, blue, and black, respectively.

4 Strengths and limitations

A key strength of this work is the physically consistent coupling between a parsimonious stochastic streamflow generator (AMA) – that preserves the HK dynamics, the second-order dependence structure, time asymmetry, and the first four 305 statistical moments of the marginal distribution – and time-dependent scour and fill models that includes both erosional and sediment (re)deposition dynamics. The latter framework enables the synthetic generation of more realistic scour time-series during the entire bridge lifespan, capturing complex hydrological dynamics and their associated behaviour in terms of erosion and fill of sediments (that equilibrium formulas cannot account for). The framework is representative at multiple 310 temporal scales: the joint use of climacogram and climacospectrum (with bias correction) quantifies roughness (M) and persistence (H), allowing for a rigorous examination of short-, intermediate- and long-term dependence and their implications for forensic scour analysis. Methodologically, the study considers a long, hourly, near-natural record from



Southern Chile, thereby improving the computation of the effective flow work and the fidelity of possible hydrological dynamics. Uncertainty was explored in a structured way: >12,000 Monte Carlo realisations across three sediment-supply scenarios (ξ) yield envelope and mean behaviours, explicitly separating sediment fill effects. Additionally, the extreme-value analysis compares scour dynamics with the equilibrium scour depth, directly informing risk-based design (e.g., exceedance probabilities of $z/z_{eq} > 1$) rather than relying on single deterministic values. Finally, transparent reproducibility (MATLAB code availability) facilitates transfer to other sites and contexts.

In terms of limitations, the hourly resolution does not resolve sub-hourly intermittency or turbulence linked to the initiation/instability of scour holes. The latter might affect the timing and peak of scour events in flash floods. On the case study side, the bridge and reach representation is simplified (single cylindrical pier, 1D approach), excluding contraction scour, debris/ice impacts, sediment armouring, complex bedforms, and explicit 3D flow-structure interactions. In terms of scour model formulations, α_d and ξ (fill model parameters) are treated with constant values that do not change on time. Long field time series of scour depth at bridges are scarce; consequently, findings' validation relies on the plausibility of hydraulics and physics, as well as comparative metrics (e.g., CSI), rather than continuous observed scour time series. Finally, site specificity (Trancura catchment hydrology) limits immediate generalisation to other hydroclimates and sediment regimes without further analysis.

5 Conclusions

This study introduced a novel framework to investigate the stochastic and non-stochastic properties of the bridge scour process by coupling a parsimonious stochastic streamflow generator with a time-dependent scour model that accounts for both erosion and sediment fill. The stochastic generator, based on the asymmetric moving average (AMA) scheme, preserves the Hurst-Kolmogorov dynamics, the second-order dependence structure, time asymmetry, and the first four statistical moments of streamflow. The time-dependent scour model (BRISENT with sediment fill extensions) allowed the simulation of realistic scour depth time series under synthetic hydrographs. Monte Carlo experiments using 12,000 realisations across multiple sediment-supply scenarios produced a rich dataset for characterising scour variability, persistence properties, and exceedance probabilities. The main findings of the study can be summarised as follows:

- **Scour is inherently stochastic:** The generated scour time series showed persistence across short, intermediate, and long temporal scales, with Hurst parameters reaching values as high as 0.86 under certain sediment-supply scenarios. This reinforces that scour dynamics cannot be adequately represented by equilibrium formulas alone.
- **Upstream sediment supply significantly alters scour statistics:** Including upstream sediment supply and sediment fill dynamics reduced variability in envelopes and altered both the persistence structure and extreme-value behaviour. Neglecting redeposition leads to an overestimation of long-term scour growth and design depths.



345

- **Equilibrium scour depth is not a reliable upper bound:** Comparisons between scour simulations and equilibrium scour estimates demonstrated that the ratio z/z_{eq} frequently exceeded unity, especially for higher return periods and elevated sediment-supply scenarios. These findings question the common practice of relying on equilibrium scour depth as a conservative design envelope.
- **Scour–streamflow synchronisation is weak:** The Critical Success Index (CSI) values between streamflow and scour extreme events ranged between 0.15 and 0.60, highlighting that not all hydrological extremes translate directly into scour extremes. This result suggests that using streamflow-based design events alone may misrepresent the actual scour hazard.

350

- **Return period interpretation is challenged under persistence:** The presence of long-term persistence implies higher uncertainty in design scour estimates, reducing the validity of classical return period concepts. Stochastic risk-based design approaches are needed.

Future research directions should focus on extending and generalising the proposed framework. First, further work is needed to validate scour simulations against long-term field observations, particularly from surveys at bridge sites. Second, 355 incorporating more complex pier geometries, contraction scour, debris and ice effects, and armouring processes would improve the realism of simulations. Third, uncertainty quantification should be advanced by adopting Bayesian or ensemble approaches that treat hydraulic, sediment, and model parameters as random variables. Finally, integration with structural fragility analysis would enable the development of risk-based scour design and maintenance strategies, linking hydrological variability to bridge failure probabilities.

360 Code and data availability

Codes and data are available in Pizarro et al. (2025): <https://doi.org/10.17605/OSF.IO/32TZB>

Author contributions

DK developed the AMA scheme. AP and OL developed the codes for time-dependent scour computation. AP prepared the paper with contributions from all co-authors.

365 Competing interests

The authors declare that they have no conflict of interest.



Disclaimer

Copernicus Publications remains neutral with regard to jurisdictional claims made in the text, published maps, institutional affiliations, or any other geographical representation in this paper. While Copernicus Publications makes every effort to 370 include appropriate place names, the final responsibility lies with the authors. Views expressed in the text are those of the authors and do not necessarily reflect the views of the publisher.

Financial support

This work was carried out with the support of The National Research and Development Agency of the Chilean Ministry of Science, Technology, Knowledge and Innovation (ANID) through grant no. FONDECYT Iniciación 11240171 and grant no. 375 FONDECYT 1221341. DK was not supported at all.

References

Arneson, L., Zevenbergen, L., Lagasse, P., and Clopper, P.: Evaluating scour at bridges, 5th ed. FHWA-HIF-12-003., Hydraulic engineering circular No. 18., Washington, DC, USA, 2012.

380 Brandimarte, L., Montanari, A., Briaud, J.-L., and D'Odorico, P.: Stochastic Flow Analysis for Predicting River Scour of Cohesive Soils, *Journal of Hydraulic Engineering*, 132, 493–500, [https://doi.org/10.1061/\(ASCE\)0733-9429\(2006\)132:5\(493\)](https://doi.org/10.1061/(ASCE)0733-9429(2006)132:5(493)), 2006.

Breusers, H. N. C., Nicollet, G., and Shen, H. W.: Local Scour Around Cylindrical Piers, *Journal of Hydraulic Research*, 15, 211–252, <https://doi.org/10.1080/00221687709499645>, 1977.

385 Briaud, J.-L., Brandimarte, L., Wang, J., and D'Odorico, P.: Probability of scour depth exceedance owing to hydrologic uncertainty, *Georisk: Assessment and Management of Risk for Engineered Systems and Geohazards*, 1, 77–88, <https://doi.org/10.1080/17499510701398844>, 2007.

Chilean Ministry of Public Works (MOP): Highways design manual (In Spanish), Santiago, Chile, 2020.

Cook, W., Barr, P. J., and Halling, M. W.: Bridge Failure Rate, *Journal of Performance of Constructed Facilities*, 29, 04014080, [https://doi.org/10.1061/\(ASCE\)CF.1943-5509.0000571](https://doi.org/10.1061/(ASCE)CF.1943-5509.0000571), 2015.

390 Dargahi, B.: Controlling Mechanism of Local Scouring, *Journal of Hydraulic Engineering*, 116, 1197–1214, [https://doi.org/10.1061/\(ASCE\)0733-9429\(1990\)116:10\(1197\)](https://doi.org/10.1061/(ASCE)0733-9429(1990)116:10(1197)), 1990.

Dimitriadis, P. and Koutsoyiannis, D.: Climacogram versus autocovariance and power spectrum in stochastic modelling for Markovian and Hurst–Kolmogorov processes, *Stoch Environ Res Risk Assess*, 29, 1649–1669, <https://doi.org/10.1007/s00477-015-1023-7>, 2015.

395 Dimitriadis, P. and Koutsoyiannis, D.: Stochastic synthesis approximating any process dependence and distribution, *Stoch Environ Res Risk Assess*, 32, 1493–1515, <https://doi.org/10.1007/s00477-018-1540-2>, 2018.



Dimitriadis, P., Koutsoyiannis, D., Iliopoulou, T., and Papanicolaou, P.: A Global-Scale Investigation of Stochastic Similarities in Marginal Distribution and Dependence Structure of Key Hydrological-Cycle Processes, *Hydrology*, 8, 59, <https://doi.org/10.3390/hydrology8020059>, 2021a.

400 Dimitriadis, P., Koutsoyiannis, D., Iliopoulou, T., and Papanicolaou, P.: A Global-Scale Investigation of Stochastic Similarities in Marginal Distribution and Dependence Structure of Key Hydrological-Cycle Processes, *Hydrology*, 8, 59, <https://doi.org/10.3390/hydrology8020059>, 2021b.

Flores-Vidriales, D., Gómez, R., and Tolentino, D.: Stochastic Assessment of Scour Hazard, *Water*, 14, 273, <https://doi.org/10.3390/w14030273>, 2022.

405 German Association for Water, Wastewater and Waste (DWA): *Merkblatt DWA-M 529: auskolkungen an pfahlartigen Bauwerksgrubungen*, Hennef, Germany: DWA, 2020.

Johnson, P. A.: Reliability-based pier scour engineering, *Journal of Hydraulic engineering*, 118, 1344–1358, 1992.

Koutsoyiannis, D.: A generalized mathematical framework for stochastic simulation and forecast of hydrologic time series, *Water Resources Research*, 36, 1519–1533, <https://doi.org/10.1029/2000WR900044>, 2000.

410 Koutsoyiannis, D.: HESS Opinions “A random walk on water,” *Hydrology and Earth System Sciences*, 14, 585–601, <https://doi.org/10.5194/hess-14-585-2010>, 2010.

Koutsoyiannis, D.: Hurst-Kolmogorov Dynamics and Uncertainty, *JAWRA Journal of the American Water Resources Association*, 47, 481–495, <https://doi.org/10.1111/j.1752-1688.2011.00543.x>, 2011.

415 Koutsoyiannis, D.: Generic and parsimonious stochastic modelling for hydrology and beyond, *Hydrological Sciences Journal*, 61, 225–244, <https://doi.org/10.1080/02626667.2015.1016950>, 2016.

Koutsoyiannis, D.: Time’s arrow in stochastic characterization and simulation of atmospheric and hydrological processes, *Hydrological Sciences Journal*, 64, 1013–1037, <https://doi.org/10.1080/02626667.2019.1600700>, 2019.

Koutsoyiannis, D.: Simple stochastic simulation of time irreversible and reversible processes, *Hydrological Sciences Journal*, 65, 536–551, <https://doi.org/10.1080/02626667.2019.1705302>, 2020.

420 Koutsoyiannis, D.: *Stochastics of Hydroclimatic Extremes - A Cool Look at Risk*, Edition 4., Kallipos Open Academic Editions, Athens, 391 pp., 2024.

Koutsoyiannis, D. and Montanari, A.: Statistical analysis of hydroclimatic time series: Uncertainty and insights, *Water Resources Research*, 43, <https://doi.org/10.1029/2006WR005592>, 2007.

425 Lee, W.-L., Lu, C.-W., and Huang, C.-K.: A Study on Interaction between Overfall Types and Scour at Bridge Piers with a Moving-Bed Experiment, *Water*, 13, 152, <https://doi.org/10.3390/w13020152>, 2021.

Link, O., Castillo, C., Pizarro, A., Rojas, A., Ettmer, B., Escauriaza, C., and Manfreda, S.: A model of bridge pier scour during flood waves, *Journal of Hydraulic Research*, 55, 310–323, <https://doi.org/10.1080/00221686.2016.1252802>, 2017.

Link, O., García, M., Pizarro, A., Alcayaga, H., and Palma, S.: Local scour and sediment deposition at bridge piers during floods, *Journal of Hydraulic Engineering*, 146, 04020003, 2020.



430 Lu, J.-Y., Hong, J.-H., Su, C.-C., Wang, C.-Y., and Lai, J.-S.: Field measurements and simulation of bridge scour depth variations during floods, *Journal of Hydraulic Engineering*, 134, 810–821, 2008.

Melville, B. and Coleman, S.: *Bridge scour*, Water Resources Publications, LLC, Littleton, CO, USA, 2000.

Meyer-Peter, E. and Müller, R.: Formulas for Bed-Load transport, IAHSR 2nd meeting, Stockholm, appendix 2, 1948.

Pizarro, A., Samela, C., Fiorentino, M., Link, O., and Manfreda, S.: BRISENT: An Entropy-Based Model for Bridge-Pier Scour Estimation under Complex Hydraulic Scenarios, *Water*, 9, 889, <https://doi.org/10.3390/w9110889>, 2017a.

Pizarro, A., Ettmer, B., Manfreda, S., Rojas, A., and Link, O.: Dimensionless Effective Flow Work for Estimation of Pier Scour Caused by Flood Waves, *Journal of Hydraulic Engineering*, 143, 06017006, [https://doi.org/10.1061/\(ASCE\)HY.1943-7900.0001295](https://doi.org/10.1061/(ASCE)HY.1943-7900.0001295), 2017b.

Pizarro, A., Manfreda, S., and Tubaldi, E.: The Science behind Scour at Bridge Foundations: A Review, *Water*, 12, 374, 440 <https://doi.org/10.3390/w12020374>, 2020.

Pizarro, A., Ettmer, B., and Link, O.: Relative importance of parameters controlling scour at bridge piers using the new toolbox ScourAPP, *Computers & Geosciences*, 163, 105117, <https://doi.org/10.1016/j.cageo.2022.105117>, 2022.

Pizarro, A., Link, O., and Koutsoyiannis, D.: Codes And Data For “Variability And Persistence Of Scour At Bridges Using Stochastic Simulations,” 2025.

445 Raudkivi, A. J.: Functional trends of scour at bridge piers, *Journal of hydraulic engineering*, 112, 1–13, 1986.

Rifo, C., Arriagada, P., Ettmer, B., and Link, O.: Frequency analysis of extreme scour depths at bridge piers and their contribution to bridge collapse risk, *Hydrological Sciences Journal*, 67, 2029–2041, <https://doi.org/10.1080/02626667.2022.2122718>, 2022.

450 Shahriar, A. R., Montoya, B. M., Ortiz, A. C., and Gabr, M. A.: Quantifying probability of deceedance estimates of clear water local scour around bridge piers, *Journal of Hydrology*, 597, 126177, <https://doi.org/10.1016/j.jhydrol.2021.126177>, 2021.

Sheppard, D. M., Melville, B., and Demir, H.: Evaluation of Existing Equations for Local Scour at Bridge Piers, *Journal of Hydraulic Engineering*, 140, 14–23, [https://doi.org/10.1061/\(ASCE\)HY.1943-7900.0000800](https://doi.org/10.1061/(ASCE)HY.1943-7900.0000800), 2014.

455